Key Points:
- The CESM2(CAM6) winter ice thickness distribution is biased thin and leads to a lower summer sea ice area than observed
- The timing of first Arctic ice-free conditions in the CESM2 is independent of the choice of CMIP6 future emissions scenario
- By 2100, CESM2 shows an accelerated decline in winter and spring area under the high emissions scenario due to reduced fall ocean heat loss

Supporting Information:
- Supporting Information S1

Correspondence to:
P. DeRepentigny,
patricia.derepentigny@colorado.edu

Arctic Sea Ice in Two Configurations of the CESM2 During the 20th and 21st Centuries

Patricia DeRepentigny[1] , Alexandra Jahn[1] , Marika M. Holland[2] , and Abigail Smith[1]

[1]Department of Atmospheric and Oceanic Sciences and Institute of Arctic and Alpine Research, University of Colorado Boulder, Boulder, CO, USA, [2]Climate and Global Dynamics Laboratory, National Center for Atmospheric Research, Boulder, CO, USA

Abstract We provide an assessment of the current and future states of Arctic sea ice simulated by the Community Earth System Model version 2 (CESM2). The CESM2 is the version of the CESM contributed to the sixth phase of the Coupled Model Intercomparison Project (CMIP6). We analyze changes in Arctic sea ice cover in two CESM2 configurations with differing atmospheric components: the CESM2(CAM6) and the CESM2(WACCM6). Over the historical period, the CESM2(CAM6) winter ice thickness distribution is biased thin, which leads to lower summer ice area compared to CESM2(WACCM6) and observations. In both CESM2 configurations, the timing of first ice-free conditions is insensitive to the choice of CMIP6 future emissions scenario. In fact, the probability of an ice-free Arctic summer remains low only if global warming stays below 1.5°C, which none of the CMIP6 scenarios achieve. By the end of the 21st century, the CESM2 simulates less ocean heat loss during the fall months compared to its previous version, delaying sea ice formation and leading to ice-free conditions for up to 8 months under the high emissions scenario. As a result, both CESM2 configurations exhibit an accelerated decline in winter and spring ice area, a behavior that had not been previously seen in CESM simulations. Differences in climate sensitivity and higher levels of atmospheric CO_2 by 2100 in the CMIP6 high emissions scenario compared to its CMIP5 analog could explain why this winter ice loss was not previously simulated by the CESM.

Plain Language Summary We provide a first look at the current and future states of Arctic sea ice as simulated by the Community Earth System Model version 2 (CESM2), which is part of the newest generation of large-scale climate models. The CESM2 model has two configurations that differ in their representation of atmospheric processes: the CESM2(CAM6) and the CESM2(WACCM6). We find several differences in the simulated Arctic sea ice cover between the two CESM2 configurations, as well as compared to the previous generation of the CESM model. Over the historical period, the CESM2(CAM6) model simulates a winter ice cover that is too thin, which leads to lower summer ice coverage compared to the CESM2(WACCM6) model and observations. In both CESM2 configurations, the probability of the Arctic becoming nearly ice free at the end of the summer remains low only if global warming stays below 1.5°C. In addition, the specific year a first ice-free Arctic is reached is not sensitive to the future greenhouse gas emissions trajectories considered here. In contrast to the previous generation of the CESM, both CESM2 configurations project an accelerated decline in winter and spring ice area by the end of the 21st century if greenhouse gases emissions remain high.

1. Introduction

In recent decades, the Arctic sea ice cover has changed dramatically, with negative linear trends in sea ice extent in all months (Stroeve & Notz, 2018). The loss of summer sea ice has been particularly striking, with decreases of roughly 50% and 66% in September ice extent and thickness since 1979, respectively (Comiso et al., 2017; Kwok, 2018; Stroeve & Notz, 2018). Newly available climate model simulations from the sixth phase of the Coupled Model Intercomparison Project (CMIP6; Eyring et al., 2016) represent a powerful tool for advancing our understanding of present and future changes in the Arctic climate system. The Sea-Ice Model Intercomparison Project (SIMIP; Notz et al., 2016) community has recently found that CMIP6 model performance in simulating Arctic sea ice is similar to CMIP5 and CMIP3 in many aspects but that the sensitivity of Arctic sea ice to changes in the forcing is generally better captured by CMIP6 models (SIMIP Community, 2020).

Author Contributions:
Conceptualization: Patricia DeRepentigny, Alexandra Jahn
Formal analysis: Patricia DeRepentigny, Marika M. Holland, Abigail Smith
Methodology: Patricia DeRepentigny, Alexandra Jahn, Marika M. Holland, Abigail Smith
Supervision: Alexandra Jahn
Writing - original draft: Patricia DeRepentigny
Writing – review & editing: Patricia DeRepentigny, Alexandra Jahn, Marika M. Holland, Abigail Smith

The Community Earth System Model version 2 (CESM2; Danabasoglu et al., 2020) is the contribution of the National Center for Atmospheric Research (NCAR) to CMIP6. Two separate CESM2 configurations that differ only in their atmosphere model have been contributed to CMIP6. The Community Earth System Model (CESM) and its various iterations have been widely used in the past to understand the changing Arctic and have performed well in capturing the Arctic mean sea ice state, trends, and variability (e.g., Barnhart et al., 2016; DeRepentigny et al., 2016; England et al., 2019; Jahn et al., 2016; Labe et al., 2018). The goal of this paper is to provide an overview of the major Arctic sea ice features in the CESM2 during the 20th and 21st centuries that are of interest to the Arctic and global climate change communities. Specifically, we assess the performance of the two CESM2 configurations over the historical period in comparison with both the previous CESM version and available observations (section 3). This is followed by an analysis of the future evolution of the Arctic sea ice cover in the two configurations, including determining when an ice-free Arctic may occur (section 4) and documenting a dramatic winter and spring ice loss in the late 21st century due to a reduction in oceanic heat loss in fall (section 5), something that had not been previously seen in the CESM model over the 21st century. Finally, we present some initial analysis of a reduction in the simulated negative trends of Arctic sea ice cover at the historical-scenario transition (section 6). The source of the differences in Arctic sea ice simulations between the two CESM2 configurations in the preindustrial simulations is analyzed in a companion paper by DuVivier et al. (2020).

2. Data and Methods

2.1. CESM2

The CESM2 is a community-developed, fully-coupled earth system model publicly available at www.cesm.ucar.edu/models/cesm2/. It is the latest generation of the CESM and NCAR's contribution to CMIP6. Two separate CESM2 configurations have been contributed to the CMIP6 effort, differing only in their atmosphere component: the "low-top" (40 km, with limited chemistry) Community Atmosphere Model version 6 (CAM6; Danabasoglu et al., 2020) and the "high-top" (140 km, with interactive chemistry) Whole Atmosphere Community Climate Model version 6 (WACCM6; Gettelman, Mills, et al., 2019). The CESM2 presents several science and infrastructure changes that have been fully documented in Danabasoglu et al. (2020). In particular, the CESM2 shows large reductions in low-latitude precipitation and shortwave cloud radiative forcing biases, resulting in improved historical simulations with respect to the available observations compared to its previous major release, the CESM1.1 (Hurrell et al., 2013). As a result of an improved cloud distribution compared to the CESM1.1, increased cloud feedbacks in the CESM2 lead to a higher equilibrium climate sensitivity (ECS; Gettelman, Hannay, et al., 2019) that is more than 1°C above the ECS of the CESM1.1 (Danabasoglu et al., 2020) and at the upper end of the range of CMIP6 models (Meehl et al., 2020).

The CESM2 uses a nominal 1° (1.25° longitude × 0.9° latitude) horizontal resolution configuration, with the Parallel Ocean Program version 2 (POP2; Smith et al., 2010) as its ocean component and the Community Land Model version 5 (CLM5; Lawrence et al., 2019) as its land component. The "low-top" CAM6 atmosphere model has 32 vertical levels, and the model top reaches into the stratosphere at 3.6 hPa. The "high-top" WACCM6 model has 70 vertical levels and a model top in the lower thermosphere at 6×10^{-6} hPa. The vertical levels in CAM6 and WACCM6 are identical up to 87 hPa. A major difference between the two atmosphere models is that WACCM6 has interactive chemistry with 228 prognostic chemical species, including an extensive representation of secondary organic aerosols (Tilmes et al., 2019). WACCM6 simulations were used to force the CAM6 simulations at the model top, so that both model configurations use the same forcing. The two CESM2 configurations will be referred to as CESM2(CAM6) and CESM2(WACCM6) hereafter.

For its sea ice component, the CESM2 uses the Los Alamos Sea Ice Model version 5.1.2 (CICE5; Hunke et al., 2015), which has the same horizontal grid as the ocean component POP2 (as decribed in Danabasoglu et al., 2012). CICE5 uses the mushy-layer thermodynamics scheme (Turner & Hunke, 2015) rather than that of Bitz and Lipscomb (1999) which was used in CICE4, the sea ice component of CESM1. Further changes in CICE5 include a salinity-dependent freezing point for seawater (Assur, 1960), a prognostic vertical profile of ice salinity, and an updated melt pond parameterization (Hunke

Table 1

Number of Ensemble Members for the Different CESM2 Simulations and the CESM-LE

	CESM2(CAM6)	CESM2(WACCM6)	CESM-LE
Historical	11	3	40
SSP1-2.6	3	1	—
SSP2-4.5	3	3	—
SSP3-7.0	3	3[a]	—
SSP5-8.5	3	3	—
RCP8.5	—	—	40

[a]Members #2 and #3 only extend to the end of 2055.

et al., 2013). In order to better represent salinity and temperature profiles in sea ice, the vertical sea ice resolution has been increased from four layers in CICE4 to eight layers in CICE5 and from one to three layers for the vertical snow resolution.

The CESM2 historical simulations extend from 1850 to 2014, with 11 ensemble members for CESM2(CAM6) (Danabasoglu, 2019a) and three for CESM2(WACCM6) (Danabasoglu, 2019i) (Table 1). Each ensemble member is branched from a random year in its respective preindustrial control simulation. The future simulations extend from 2015 to 2100 and follow the Shared Socioeconomic Pathways (SSPs; O'Neill et al., 2014), a new scenario framework designed to account for future socio-economic development in addition to climate change resulting from increasing greenhouse gas emissions. Currently, CESM2 simulations following four different SSPs are available (Danabasoglu, 2019b, 2019c, 2019d, 2019e, 2019j, 2019k, 2019l, 2019m), and the number of ensemble members for each of the different simulations is given in Table 1. Most of the analysis presented in this paper is done using the historical and SSP5-8.5 (high challenges for mitigation and low challenges for adaptation, as described in O'Neill et al., 2016) simulations, unless noted otherwise. Note that even though the CMIP5 Representative Concentration Pathway 8.5 (RCP8.5; Van Vuuren et al., 2011) and the CMIP6 SSP5-8.5 scenarios are designed to result in the same radiative forcing when applied in a simple climate model (O'Neill et al., 2016), the prescribed concentration of greenhouse gases, land use change, and other external forcings differ substantially between the two. Notably, the SSP5-8.5 scenario reaches higher atmospheric CO_2 concentration by the end of the century (see Figure 3 of O'Neill et al., 2016). The different transient nature of the forcings and different radiative feedbacks in the models will influence the radiative imbalance at the top of the atmosphere that results by 2100. Hence, some combination of differences in the forcing and the higher ECS in the CESM2 compared to the CESM1 (Gettelman, Hannay, et al., 2019) leads to an additional 1°C of warming in the CESM2 compared to the CESM1 by the end of the 21st century (Meehl et al., 2020).

Note that here we use the CESM2(CAM6) future scenario simulations contributed to the CMIP6 archive in May 2020. The initial CESM2(CAM6) future scenario simulations submitted to the CMIP6 archive had to be retracted in April 2020 because anthropogenic and biomass burning secondary organic aerosol emissions were set to zero starting in 2015 in error and have been replaced by the new runs analyzed here. For Arctic sea ice, no impact of this erroneous forcing in the future scenario simulations is detectable within the limits of internal variability, so any results based on the previous CESM2(CAM6) Arctic sea ice output remain valid (e.g., SIMIP Community, 2020) but will differ in their internal variability from the new set of runs shown here.

We use sea ice area as our primary variable to describe sea ice coverage instead of extent since sea ice extent is a strongly grid-dependent, nonlinear quantity, making model comparisons less accurate (Notz, 2014). Note however that we use sea ice extent in section 4 where we discuss ice-free conditions in the Arctic to allow for comparison with previous studies that all define ice-free conditions in terms of ice extent. An assessment of the effect of using extent rather than area to define ice-free conditions is provided in section 4.

2.2. CESM Large Ensemble

Results from the CESM2 simulations are compared to the previous version of the CESM, the CESM1.1-CAM5 (Hurrell et al., 2013). In particular, we use the CESM Large Ensemble (CESM-LE; Kay et al., 2015), a 40-member ensemble experiment (Table 1) that has been widely used for Arctic sea ice studies and generally performs well when compared to observations (e.g., Barnhart et al., 2016; DeRepentigny et al., 2016; England et al., 2019; Jahn et al., 2016; Kirchmeier-Young et al., 2017; Smith, & Jahn, 2019; Swart et al., 2015). It follows the RCP8.5 scenario with the same radiative imbalance by 2100 as the SSP5-8.5 scenario used to force the CESM2. The CESM-LE historical simulations span 1920 to 2005, while the RCP8.5 simulations cover 2006 to 2100.
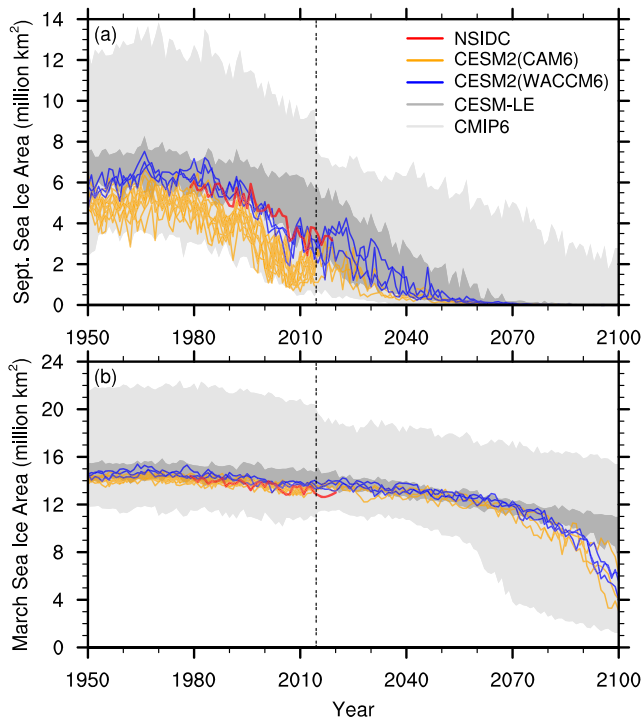
Figure 1. Time evolution of (a) September and (b) March Arctic sea ice area in the observations (red), the CESM2(CAM6) (orange), the CESM2(WACCM6) (blue), the CESM-LE (dark gray), and the CMIP6 model spread (light gray). The vertical double-dashed lines indicate the transition year between historical and future simulations in CMIP6. Note that the reduction of the spread across CMIP6 models at the historical-scenario transition is due to a lower number of available simulations under the SSP5-8.5 scenario compared to historical simulations. The CMIP6 range shown here is the same as in SIMIP Community (2020).

2.3. Observational Data Sets for Comparison

To assess how realistic the CESM2 simulations are in terms of Northern Hemisphere monthly sea ice area over the satellite era, we use the National Snow and Ice Data Center (NSIDC) Sea Ice Index version 3 (Fetterer et al., 2017) between 1979 and 2020, with the observational pole hole filled assuming sea ice concentration of 100%. We also use sea ice concentration data derived from passive microwave brightness temperature from the National Oceanic and Atmospheric Administration (NOAA)/NSIDC Climate Data Record (Meier et al., 2017; Peng et al., 2013) to identify the location of the observed sea ice edge (defined as the 15% sea ice concentration contour). For the analysis of sea ice thickness, we do not compare model results to reanalyzed or observational estimates as those still exhibit substantial uncertainties (Bunzel et al., 2018; Chevallier et al., 2017).

3. Historical Arctic Sea Ice

3.1. September—Arctic Sea Ice Minimum

Over the historical period, the simulated September pan-Arctic sea ice cover differs greatly between the CESM2(CAM6) and the CESM2 (WACCM6) (Figures 1a and 2a–2f). The September ice area in CESM2 (WACCM6) compares well with observations over the satellite era (Figures 1a and 2d–2f). Conversely, the CESM2(CAM6) September ice area is consistently lower than observed (Figure 1a), with too little ice in the Pacific and Eurasian sectors of the Arctic (Figures 2a–2c). DuVivier et al. (2020) found that differences in ice area already exist between CESM2(CAM6) and CESM2(WACCM6) in their preindustrial control simulations, with the largest differences in the summer months. These discrepancies in ice area and volume can be attributed to thinner early spring clouds in the CESM2(CAM6), which drive a strong ice-albedo feedback and result in a lower ice area in September and significantly thinner ice year-round (DuVivier et al., 2020). Compared to the spread of the CESM-LE, the CESM2(CAM6) September sea ice area is consistently less
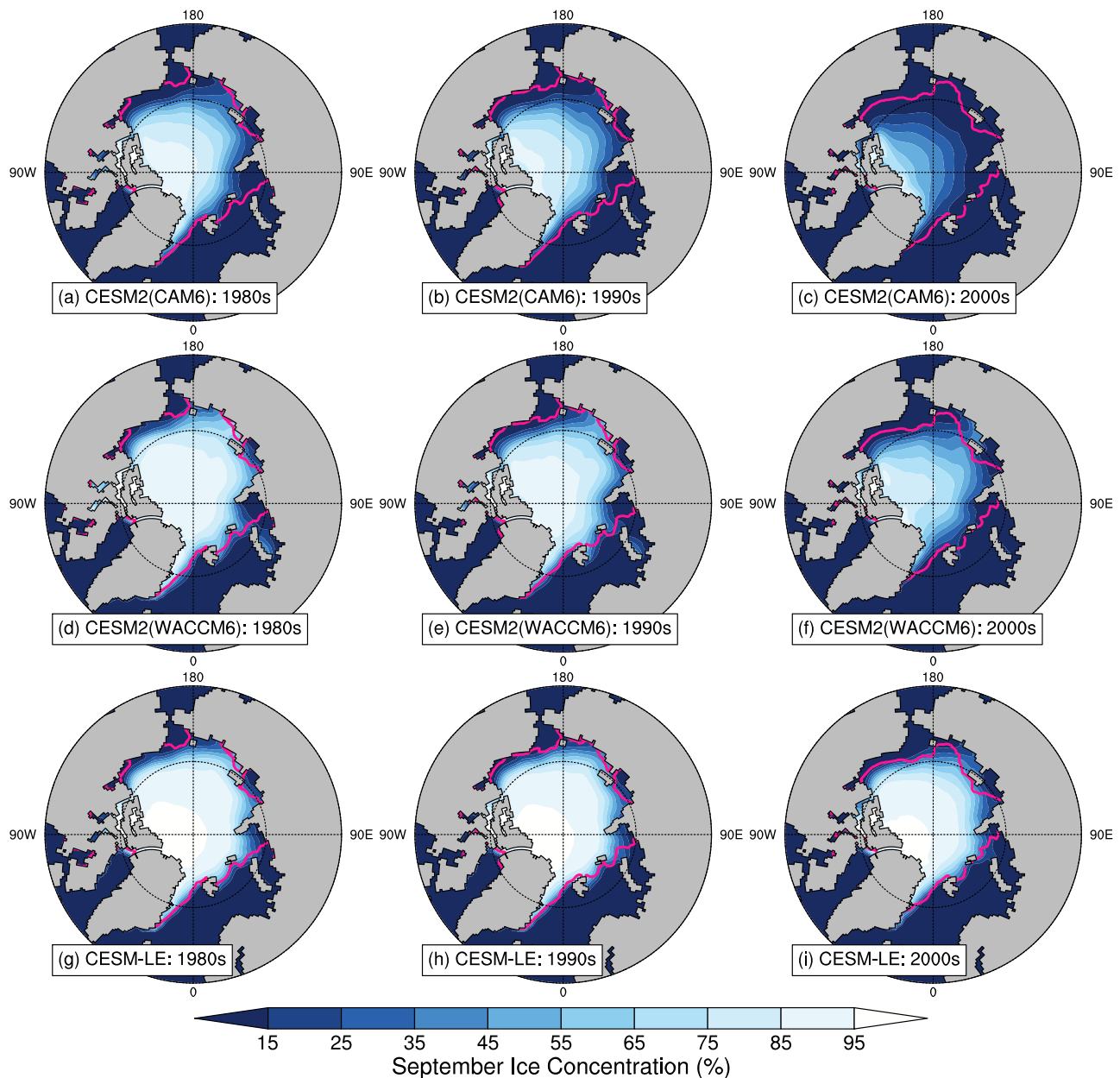
extensive, while the CESM2(WACCM6) sea ice area falls at the low end of the range of internal variability of the CESM-LE (Figure 1a). Compared to the available CMIP6 simulations (SIMIP Community, 2020), the CESM2(CAM6) falls at the low end of the spread while the CESM2(WACCM6) is found in the lowest one third of the CMIP6 model spread (Figure 1a).

The decline in summer ice area at the end of the 20th century occurs more rapidly in the CESM2 (Figures 2a–2f) than in the CESM-LE (Figures 2g–2i) and results in a Northern Hemisphere September sea ice area for the CESM2(WACCM6) that compares more favorably to observations at the start of the 21st century (Figure 1a). The CESM2(CAM6) sea ice coverage (Figures 2a–2c) is consistently less extensive than the CESM2(WACCM6) and the CESM-LE almost everywhere in the Arctic, with no ice left in the peripheral seas at the end of the summer. By the 2000s, sea ice is confined to the Central Arctic in the CESM2(CAM6), with open-water conditions over a large area of the Pacific, Eurasian, and Atlantic sectors of the Arctic Ocean.

3.2. March—Arctic Sea Ice Maximum

At the Arctic sea ice maximum in March, sea ice area is comparable to observations in both CESM2 configurations, whereas it is generally too extensive in the CESM-LE (Figure 1b). The lower March sea ice area in the CESM2 compared to the CESM-LE is mainly due to less ice coverage in the Pacific Ocean south of the Bering Strait (not shown), and these differences in winter ice coverage between the two model versions get larger toward the end of the historical period (Figure 1b).

Figure 2. Ensemble mean, decadal mean September sea ice concentration during the 1980s (a, d, g), 1990s (b, e, h), and 2000s (c, f, i) in the CESM2(CAM6) (a–c), the CESM2(WACCM6) (d–f), and the CESM-LE (g–i). The decadally averaged observed sea ice edge (defined as the 15% sea ice concentration contour) is indicated by the pink line.

In addition to ice area, an accurate representation of winter ice thickness is important to effectively characterize the sea ice state in light of the inverse relationship between sea ice volume and the efficiency of thermodynamic processes such as sea ice growth and melt (Bitz & Roe, 2004). This relationship impacts the simulated Arctic sea ice volume variability on long time scales and thus the projected evolution of Arctic sea ice (Massonnet et al., 2018). Compared to 5 years of gridded ICESat satellite sea ice thickness data in February and March (2003–2007), DuVivier et al. (2020) found that the CESM2(WACCM6) agrees better with observations than the CESM2(CAM6), despite ICESat observations showing a higher fraction of thick ice (>2 m) than both CESM2 configurations (see their Figure 4a). We find that during the 1980s, the CESM2(CAM6) March ice thickness distribution is biased thin compared to the CESM2(WACCM6) and the CESM-LE (Figure 3a). In particular, the CESM2(CAM6) distribution is unimodal, with a peak in ice
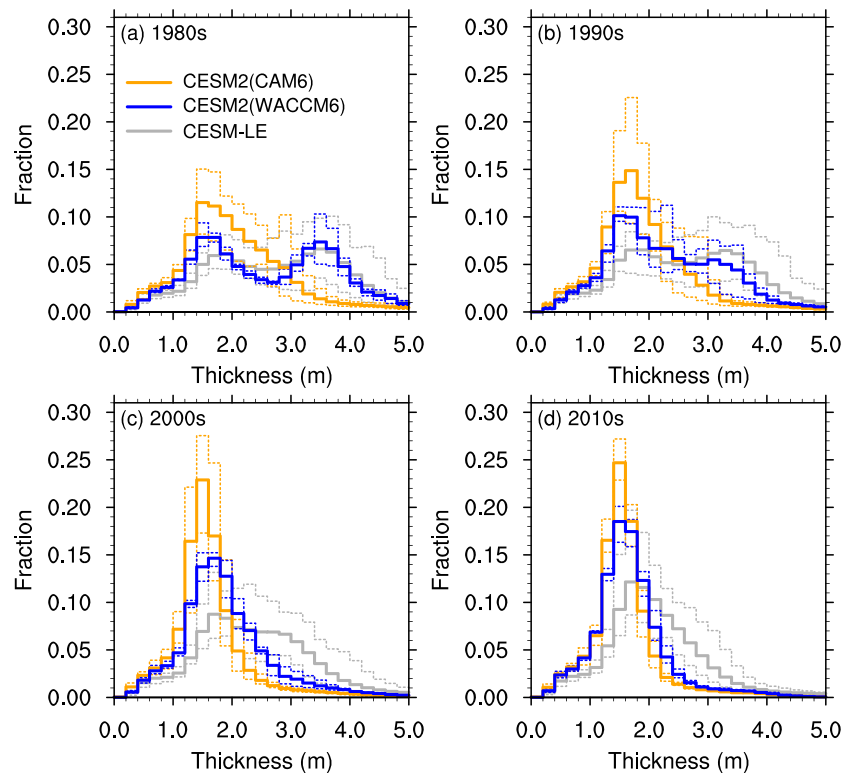
Figure 3. Fraction of total March ice area (where ice concentration is greater or equal to 15%) for different ice thickness categories during the (a) 1980s, (b) 1990s, (c) 2000s, and (d) 2010s in the CESM2(CAM6) (orange), the CESM2(WACCM6) (blue), and the CESM-LE (gray). The solid line and the lower/upper dotted lines show the mean and the minimum/ maximum across all ensemble members, respectively. In panel (d), given the different number of ensemble members in the historical (2010–2014) and the SSP5-8.5 (2015–2019) simulations of the CESM2(CAM6), only ensemble members that cover the full decade are used.

thickness at ~1.5 m and an asymmetric tail toward thicker ice. This unimodal structure is also present during the early 20th century of the CESM2(CAM6) historical simulations (not shown). On the other hand, the CESM2(WACCM6) and the CESM-LE have similar, bimodal ice thickness distributions (Figure 3a) with a high percentage of thin ice (ranging from 1.2–2.0 m) and a similarly high percentage of thick ice (ranging from 3.0–4.0 m). The shape of the ice thickness distribution in the CESM2(CAM6) is associated with a low winter mean sea ice thickness, with a sea ice cover up to 1.5 m thinner over most of the Arctic Ocean compared to the CESM2(WACCM6) and the CESM-LE (Figures 4a, 4d, and 4g).

During the 1990s, the CESM2(WACCM6) gains ice in the thinner categories at the expense of the thicker categories, whereas the CESM-LE retains its characteristic bimodal shape with similar fractions of ice across the two modes (Figure 3b). The loss of thick ice (>3 m) in the CESM2(WACCM6) occurs mainly over the Central Arctic (Figure 4e). For the CESM-LE, the loss of thick ice over the Central Arctic begins in the 2000s, reaching a similar winter state as the CESM2(WACCM6) a decade later on average (Figures 3b, 3c, 4e, and 4i). At the start of the 21st century, the CESM2(WACCM6) exhibits a unimodal shape similar to the CESM2(CAM6), but with the peak of the distribution slightly shifted toward thicker ice categories (Figure 3c). By the 2010s, all three model simulations show substantially reduced fractions of ice thicker than 3 m, with the peak of each distribution centered around ice thicknesses of 1–2 m (Figure 3d).

4. Ice-Free Conditions

In both CESM2 configurations, we find that the timing of first summer ice-free conditions (defined as pan-Arctic monthly sea ice extent below 1 million km^2) is insensitive to the choice of future emissions scenario considered here (i.e., SSP1-2.6, SSP2-4.5, SSP3-7.0, and SSP5-8.5; Figure 5a). The absence of a
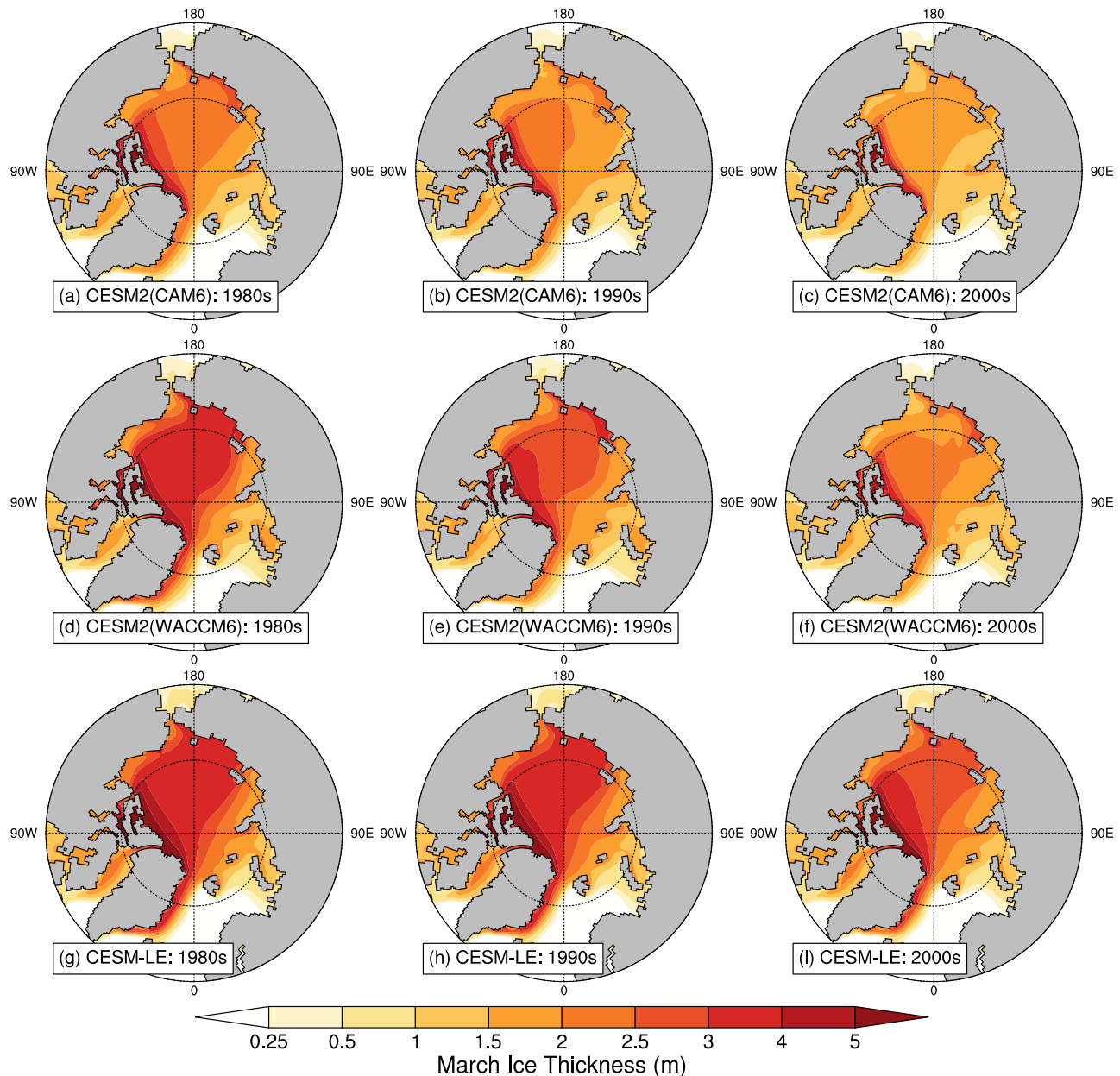
Figure 4. Ensemble mean, decadal mean March ice thickness during the 1980s (a, d, g), 1990s (b, e, h), and 2000s (c, f, i) in the CESM2(CAM6) (a–c), the CESM2(WACCM6) (d–f), and the CESM-LE (g–i). Note that the spacing of the color shading is uneven to highlight the thinner ice categories.

relationship between the year of first September ice-free conditions and the different SSPs in the CESM2 implies that internal variability, not differences in future anthropogenic emissions as represented by the CMIP6 future scenarios, ultimately determines the year of first ice-free conditions in the Arctic. This is in agreement with an earlier study using the CESM1.1 (Jahn, 2018), as well as with the CMIP6 models overall (SIMIP Community, 2020). The lack of a scenario impact on the timing of a first ice-free Arctic can be explained by the fact that the atmospheric CO_2 concentration and resulting global mean temperature change from the different SSPs only start to substantially diverge between 2040 and 2060 (see Figure 3 of O'Neill et al., 2016), after the Arctic has already become ice free in September in the CESM2 and most CMIP6 models (SIMIP Community, 2020). Furthermore, as the mean sea ice state approaches ice-free conditions, the importance of internal variability has been shown to increase relative to the forced change necessary to melt the remaining sea ice cover in September (Jahn et al., 2016).
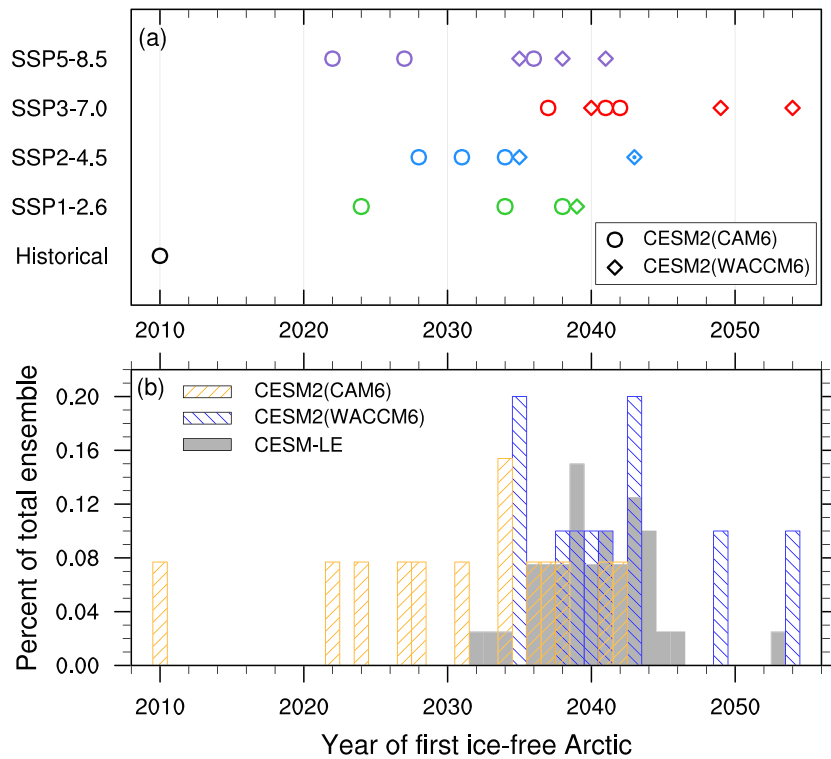
Figure 5. Timing of first ice-free Arctic: (a) Year of first September ice-free conditions in the CESM2(CAM6) (circles) and the CESM2(WACCM6) (diamonds) over the historical period (black) and the different future emissions scenarios (colors). The symbols with a dot in the middle indicate that two ensemble members reach first ice-free conditions in the same year. (b) Percentage of the total number of ensemble members reaching first September ice-free conditions in a given year in the CESM2(CAM6) (orange; total of 13 ensemble members), the CESM2(WACCM6) (blue; total of 10 ensemble members), and the CESM-LE (gray; total of 40 ensemble members). For the CESM2(CAM6) and the CESM2(WACCM6), this is done by combining the historical and all future simulations into one single distribution.

Given that we find no CMIP6 scenario impact on the timing of first ice-free conditions in September, the CESM2 simulations from each configuration can be combined to obtain a distribution of the year of first September ice-free conditions (Figure 5b). Consistent with a lower mean sea ice state, the CESM2(CAM6) generally reaches ice-free conditions earlier than the CESM2(WACCM6), with the first ice-free year occurring in 2010 for one of the CESM2(CAM6) ensemble members and in 2035 for two CESM2(WACCM6) ensemble members (Figure 5b). Despite this 25 year difference in their first ice-free year, the distributions of first September ice-free conditions in both CESM2 configurations overlap with each other, as well as with the range of the CESM-LE. The internal variability uncertainty on the year of first September ice-free conditions spans 32 and 19 years for the CESM2(CAM6) and the CESM2(WACCM6) ensembles, respectively, compared to 21 years of internal variability prediction uncertainty for the CESM-LE (Figure 5b; see also Jahn et al., 2016).

Despite seeing no impact of the choice of CMIP6 future emissions scenario on the first year of an ice-free Arctic, we still find a relatively low probability of a September ice-free Arctic in a given year in the CESM2 if global warming is limited to 1.5°C rather than 2.0°C (Figure 6b), in agreement with previous studies (Jahn, 2018; Sanderson et al., 2017; Sigmond et al., 2018). In the CESM2(CAM6), the probability of September ice-free conditions in a given year for an annual mean global temperature anomaly of 1.5°C is 6.1%, compared to 0% in the CESM2(WACCM6) and the CESM-LE (Figure 6b). For a global warming of 2.0°C, the probability of ice-free conditions in a given year increases to 83% in the CESM2(CAM6), compared to 7.0% in the CESM2(WACCM6) and 22% in the CESM-LE. These ice-free probabilities for 2.0°C of warming in the two CESM2 configurations bracket the probabilities found in previous studies for warming limited to 2.0°C, which vary between 16% and 34% (Jahn, 2018; Sanderson et al., 2017; Sigmond et al., 2018). All model simulations predict a nearly 100% chance of September ice-free conditions in a given year for 3.0°C
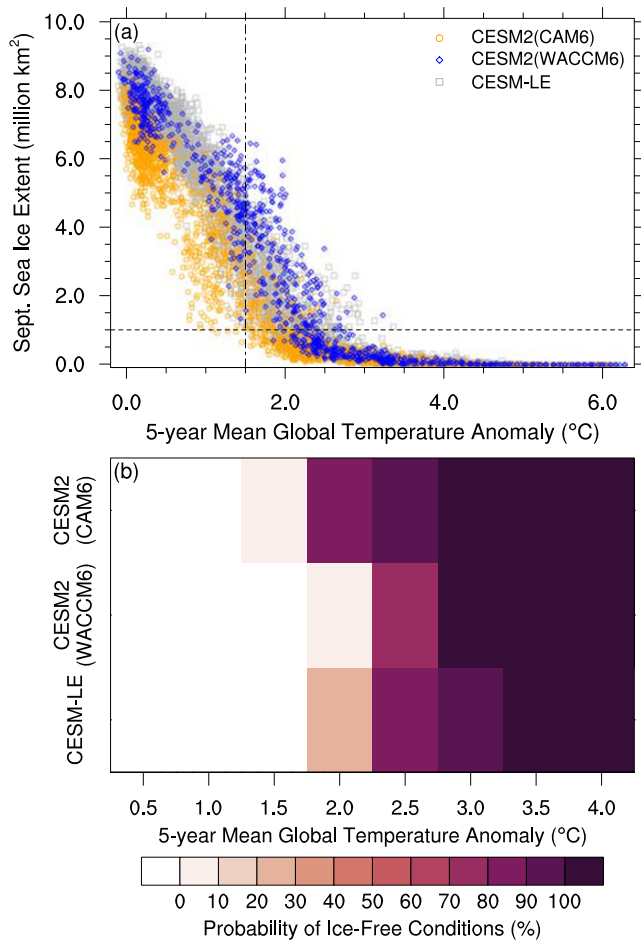
Figure 6. Ice-free Arctic as a function of global warming: (a) September sea ice extent as a function of 5-year annual mean global temperature anomaly in the CESM2(CAM6) (orange circles), the CESM2(WACCM6) (blue diamonds), and the CESM-LE (gray squares) over the historical period and the different future emissions scenarios. The horizontal dashed line indicates ice-free conditions of 1 million km^2, and the vertical dash-dotted line indicates 1.5°C of global warming. (b) Probability of September ice-free conditions for different values of 5-year annual mean global temperature anomaly in the CESM2(CAM6) (top), the CESM2(WACCM6) (middle), and the CESM-LE (bottom). The probability is calculated for temperature anomalies within ±0.1°C of each target level of warming. All temperatures shown here use the 2-m air temperature variable output, and temperature anomalies are calculated with respect to each ensemble member's 1850–1920 average.

of global warming (Figure 6b), similar to the probability of 90–100% found by Sigmond et al. (2018) using indirectly constrained 3°C stabilized warming simulations. The higher probabilities of ice-free conditions in the CESM2(CAM6) can be explained by generally lower September sea ice extent for any 5-year annual mean global temperature anomaly in this configuration compared to all other model simulations analyzed here (Figure 6a), a result of the lower winter ice thickness at the end of the historical period (see Figures 4a–4c and section 3.2).

Note that here we calculate the probability of ice-free conditions in September for 5-year annual mean global temperature anomalies within ±0.1°C of different levels of warming using every year of the historical and future simulations. This method differs from previous studies (Jahn, 2018; Sanderson et al., 2017; Screen & Williamson, 2017; Sigmond et al., 2018), which themselves all differ in their methodology. To quantify the effect of the method choice on the probabilities found, we apply our methodology to the same set of CESM1.1 stabilization experiments previously used in Jahn (2018) and Sanderson et al. (2017). We find that the probabilities are comparable but slightly lower when using our method: 0.7% versus 2.5% for 1.5°C of warming and 30% versus 34% for 2.0°C of warming. Furthermore, we find that our method yields comparable though slightly lower ice-free probabilities in a given year using transient versus stabilization simulations from the same model (the CESM1.1): 0% versus 0.7% for 1.5°C of warming and 22% versus 30% for 2.0°C of warming, respectively. This is consistent with the expectation that transient simulations likely underestimate the true probability of ice-free conditions for a climate around a specific value of global warming, due to an inadequate sampling of internal variability (Jahn, 2018; Screen, 2018; Sigmond et al., 2018) and the potential impact of a delayed oceanic response to atmospheric warming on sea ice (Gillett et al., 2011; Sigmond et al., 2018). At the same time, these comparisons show that our method to assess ice-free conditions provides probabilities within 10% of previously used methods and between transient and stabilization experiments. As such, our method may be a useful technique to assess ice-free probabilities in a given year in transient simulations, in particular in the absence of stabilization experiments.

When using sea ice area rather than extent to define ice-free conditions (as done in SIMIP Community, 2020), the 1 million km^2 threshold is crossed earlier. As a result, the probabilities of ice-free conditions in a given year using sea ice area are about twice what we show here for a warming of up to 2.0°C, with smaller differences between an extent-based and an area-based threshold as the probabilities increase for larger warming. Hence, despite differences in methodology, the CESM2 results are overall consistent with previous studies that showed that by limiting global warming to 1.5°C, the probability of Arctic ice-free conditions in a given year is low, increases for a warming of 2.0°C, and can be expected every year for a warming of 3.0°C or more (Jahn, 2018; Sigmond et al., 2018).

5. Accelerated Decline in Winter and Spring Ice Cover

Toward the end of the 21st century, both CESM2 configurations simulate an accelerated decline in sea ice area during the winter and spring months (Figure 7). This winter and spring ice loss is not seen in the previous version of the CESM and results in monthly ice area values that fall significantly below the range of internal variability of the CESM-LE (Figure 7). Both CESM2 configurations even simulate ice-free conditions for up to 8 months per year by 2100, with only the months of February to May showing a pan-Arctic ice extent larger than 1 million km^2 (not shown) compared to a maximum of five months of ice-free
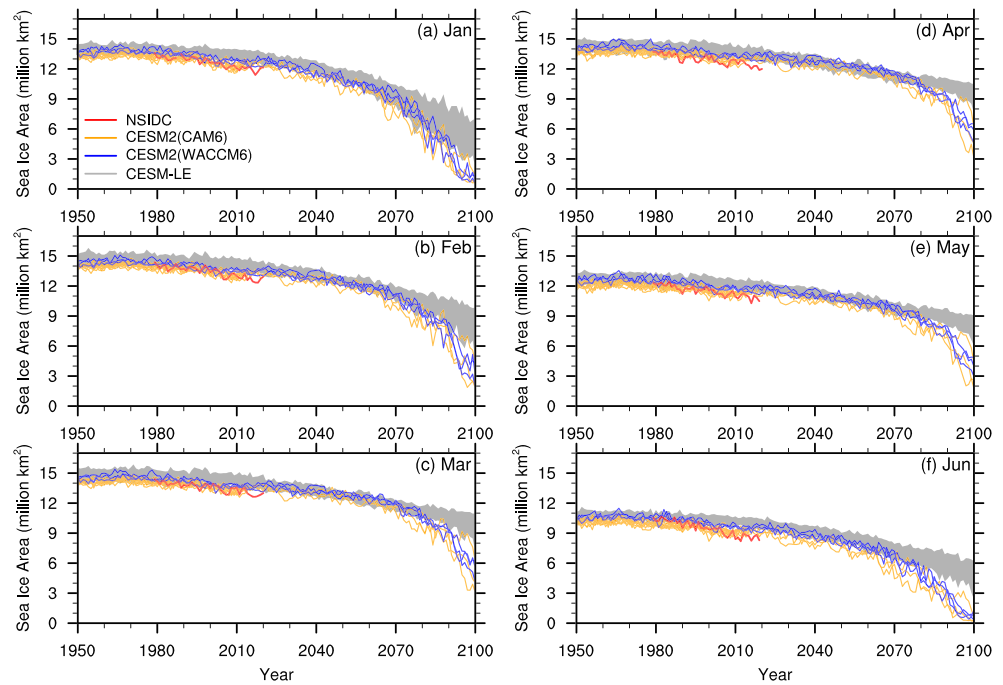
Figure 7. Time evolution of Arctic sea ice area from January to June (a–f) in the observations (red), the CESM2(CAM6) (orange), the CESM2(WACCM6) (blue), and the CESM-LE (gray).

conditions for the CESM-LE (Jahn, 2018). Some other CMIP6 models show a similar acceleration of the March sea ice area decline over the last 20–30 years of the 21st century (see Figure 2c of SIMIP Community, 2020). The retreat of March ice area originates in the Chukchi Sea in the 2070s in the CESM2(CAM6) and the 2080s in the CESM2(WACCM6), leaving a large portion of the Pacific sector of the Arctic ice free by the 2090s (Figures 8a–8f). The CESM-LE only starts to show a similar winter ice loss in the Chukchi Sea at the end of the century, lagging the CESM2(CAM6) by two decades and the CESM2(WACCM6) by one decade (Figures 8g–8i). This lag between the different model versions is consistent with a similarly delayed response of winter ice thickness over the historical period (Figure 4).

The discrepancies in the time evolution of winter and spring ice area between the two CESM versions (Figure 7) arise as the CESM2 reaches a very different climate at the end of the 21st century compared to the CESM-LE. Despite the same top-of-atmosphere radiative forcing in the SSP5-8.5 and RCP8.5 scenarios in 2100, the SSP5-8.5-forced CESM2 simulates higher annual Arctic (and global) temperatures by 2100 compared to the RCP8.5-forced CESM-LE (Figure 9b). These higher temperatures are likely a result of the higher ECS in the CESM2 compared to the CESM-LE (Gettelman, Hannay, et al., 2019; Meehl et al., 2020) as well as differences in the applied forcing. When considering the evolution of March ice area as a function of CO_2 concentration, the CESM2 largely falls within the range of internal variability of the CESM-LE (Figure 9a). Similar results are found for the evolution of March sea ice area as a function of annual Arctic temperature (Figure 9b). However, toward the end of the CESM-LE simulations (i.e., around CO_2 concentrations of 900 ppm and annual mean Arctic temperatures of $-4°C$), the approximately linear relationship between March sea ice area and atmospheric CO_2 and Arctic temperature breaks down as the CESM2 reaches a considerably warmer climate than the CESM-LE (Figures 9a and 9b). This points to a non-linear behavior of winter Arctic sea ice area that was not sampled in the CESM-LE. Due to the differences in greenhouse gas trajectories and climate sensitivities between CMIP5 and CMIP6, comparing simulated sea ice properties as a function of CO_2 concentration or temperature rather than time is found to be a more appropriate way to assess differences in sea ice evolution. However, care should be taken when comparing model versions with different climate base states in terms of temperature anomaly rather than absolute temperature. We find that while the evolution of March sea ice area as a function of Arctic temperature is consistent across the three CESM simulations (Figure 9b), it is not the case when assessed in terms of Arctic
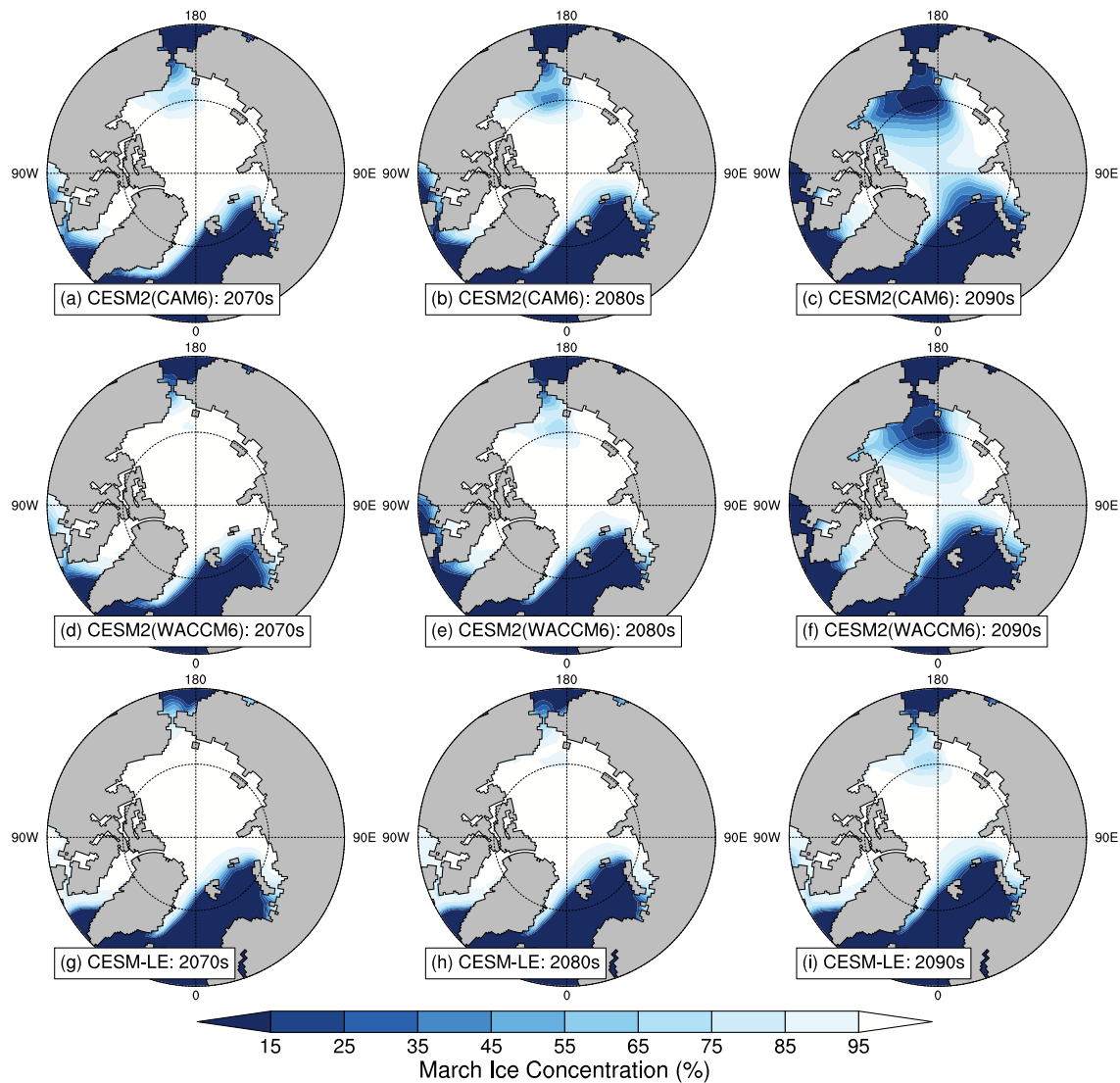
Figure 8. Ensemble mean, decadal mean March ice concentration during the 2070s (a, d, g), 2080s (b, e, h), and 2090s (c, f, i) in the CESM2(CAM6) (a–c), the CESM2(WACCM6) (d–f), and the CESM-LE (g–i).

temperature anomaly (Figure 9c). The evolution of March sea ice area as a function of annual Arctic temperature anomaly generally only overlaps with the lower end of the range of the CESM-LE, which means that the CESM2 simulates a less extensive winter ice cover for the same annual Arctic temperature anomaly (Figure 9c). This is due to the fact that the annual Arctic mean temperature of the reference period 1850–1920 used to calculate temperature anomalies is higher by about 3°C in the CESM2 compared to the CESM-LE (McIlhattan et al., 2020). As such, a smaller temperature anomaly in the CESM2 compared to the CESM-LE for the same March ice area does not correspond to a lower absolute temperature in the CESM2 if the difference in temperature anomalies is smaller than the difference in the mean temperatures of the reference period.

The accelerated decline in winter and spring ice cover in the CESM2 compared to the CESM-LE is driven in large part by changes in ocean heat loss during the preceding fall. As the Arctic goes ice free every summer in all three CESM simulations in the late 21st century, differences in winter ice area are related to the amount of ice formed during fall and winter. Before ice formation can commence in the fall, all of the mixed layer heat accumulated over the summer must be released to the atmosphere for the surface temperature of the ocean to drop below the freezing point of seawater. Similar sea surface temperatures at the sea ice
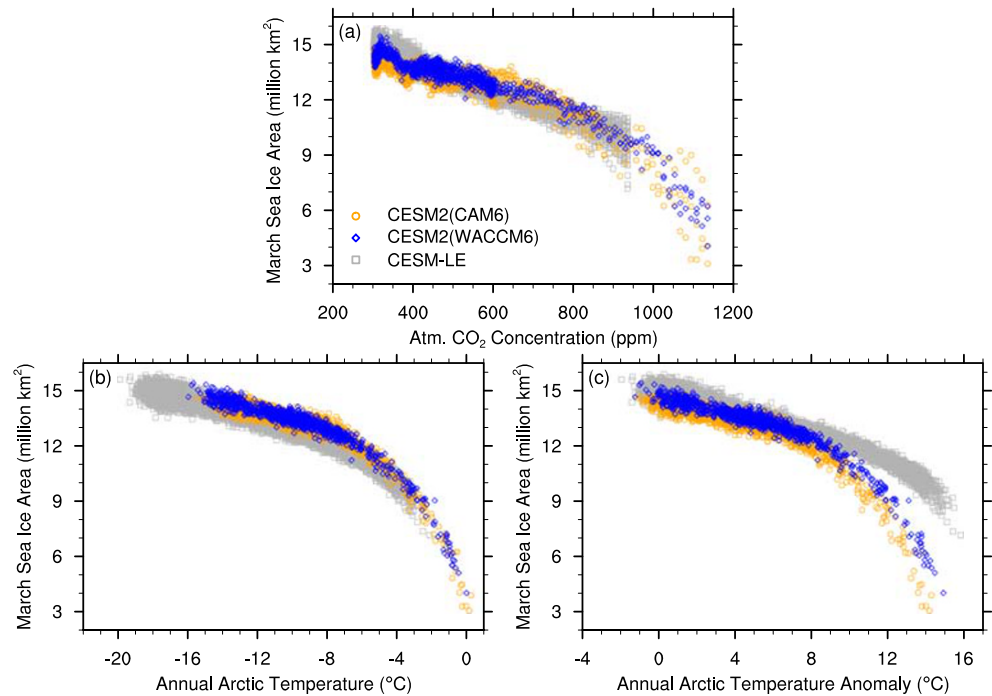
Figure 9. March sea ice area as a function of (a) annual global atmospheric CO_2 concentration, (b) annual Arctic temperature, and (c) annual Arctic temperature anomaly over the historical period and all future emissions scenarios for the CESM2(CAM6) (orange circles), the CESM2(WACCM6) (blue diamonds), and the CESM-LE (gray squares). Arctic temperatures are calculated over the region north of 70°N, and temperature anomalies are calculated with respect to each ensemble member's 1850–1920 average. All temperatures shown here use the 2-m air temperature variable output.

minimum (Figures S1a, S1e, and S1i in the supporting information) and no significant differences in volume and heat transports through the Bering Strait between the CESM2 and the CESM-LE in the late 21st century (not shown) suggest that the mixed layer heat accumulated over the summer is similar across the simulations. Hence, differences in ice formation result mainly from differences in the rate of oceanic heat loss in the fall. Indeed, we find that the ocean loses less heat to the atmosphere during the fall months in the CESM2 compared to the CESM-LE over the last two decades of the 21st century (Figure 10), preventing the formation of sea ice in the CESM2 by keeping most of the Arctic Ocean at temperatures above freezing (Figure S1). The reduced ocean heat loss in the CESM2 is related to warmer Arctic air temperatures and a reduced air-sea temperature gradient compared to the CESM-LE (Figure 9b).

As a result of the late 21st century reduction in winter and spring ice area in the CESM2, the pan-Arctic open-water period is about 1 to 2 months longer than in the CESM-LE (Figure 11). Compared to monthly mean sea ice area, the open-water period is a more practical metric for stakeholders who rely on predicted ice-free conditions (Barnhart et al., 2016; Parkinson, 2014). The open-water period is defined as the total number of days at each grid point between 1 March and 28 February of the next year when sea ice is not present, using a 15% sea ice concentration threshold to define the presence or absence of sea ice (Bliss et al., 2019). Over most of the Arctic basin, the CESM2 open-water period varies between 200 and 365 days in the 2090s (Figures 11c and 11f), in contrast to an open-water period of 140 to 240 days in the CESM-LE for the same period (Figure 11i). A later sea ice freeze-up is found to contribute more to the overall lengthening of the open-water period in the CESM2 than an earlier sea ice break-up (Figures S2 and S3), consistent with previous work (Wang et al., 2018) and with the reduced ocean heat loss found during the fall (Figure 10). Indeed, sea ice break-up occurs about 15 days earlier across the whole Arctic basin in the CESM2 compared to the CESM-LE over the last three decades of the 21st century (Figure S2), whereas sea ice freeze-up occurs up to 1 month later (Figure S3). Such a lengthening of the open-water period would have tremendous impacts on the Arctic climate system, from changes in regional oceanic heat budgets to
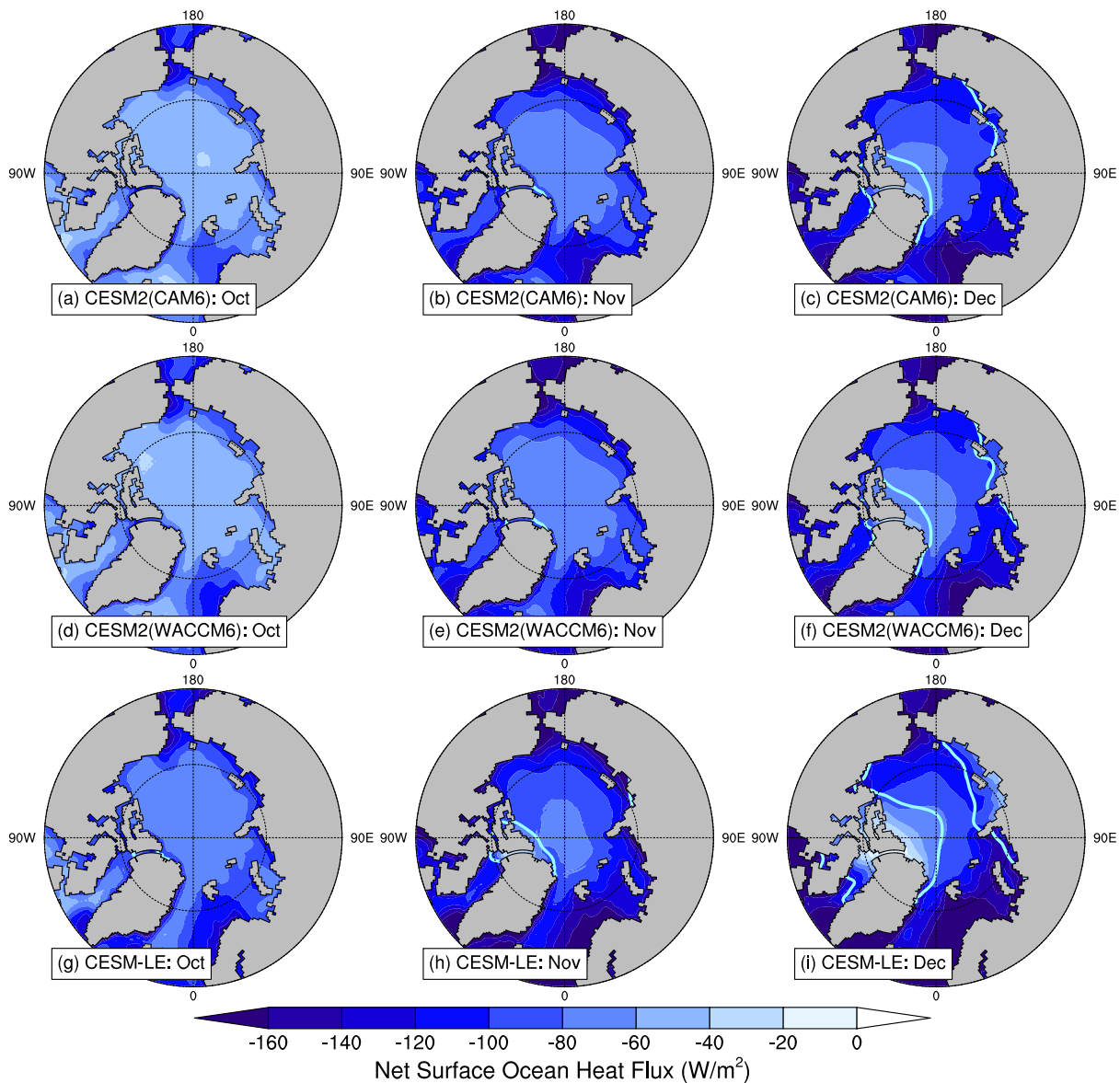
Figure 10. Ensemble mean net surface ocean heat flux averaged over 2080 to 2099 for the months of October (a, d, g), November (b, e, h), and December (c, f, i) in the CESM2(CAM6) (a–c), the CESM2(WACCM6) (d–f), and the CESM-LE (g–i). Negative values indicate heat loss from the ocean to the atmosphere. The cyan line indicates the monthly mean 15% sea ice concentration contour averaged over the same years and all ensemble members. No cyan line in a panel indicates that if there is any sea ice, sea ice concentration is below 15% everywhere.

modification of the timing of phytoplankton blooms and a shortening of the primary hunting season of large animals such as walruses, seals, and polar bears (Fernández-Méndez et al., 2015; Moore & Huntington, 2008; Perovich et al., 2007; Post et al., 2013; Stroeve et al., 2014).

6. Sea Ice Trends at the Historical-Scenario Transition

Around the transition between historical and future simulations, we find that the 20-year linear trends in September sea ice area in the CESM2 change abruptly from strongly negative to zero or even slightly positive (Figure 12; end years 2010–2025). This behavior is present in all ensemble members of both the CESM2(CAM6) and the CESM2(WACCM6) and across all future emissions scenarios (Figure 12), but not in the CESM-LE (Figures 12d and 12h; gray shading). It also appears in all months of the year, although it is most pronounced in the months surrounding the sea ice minimum (August–October) when negative
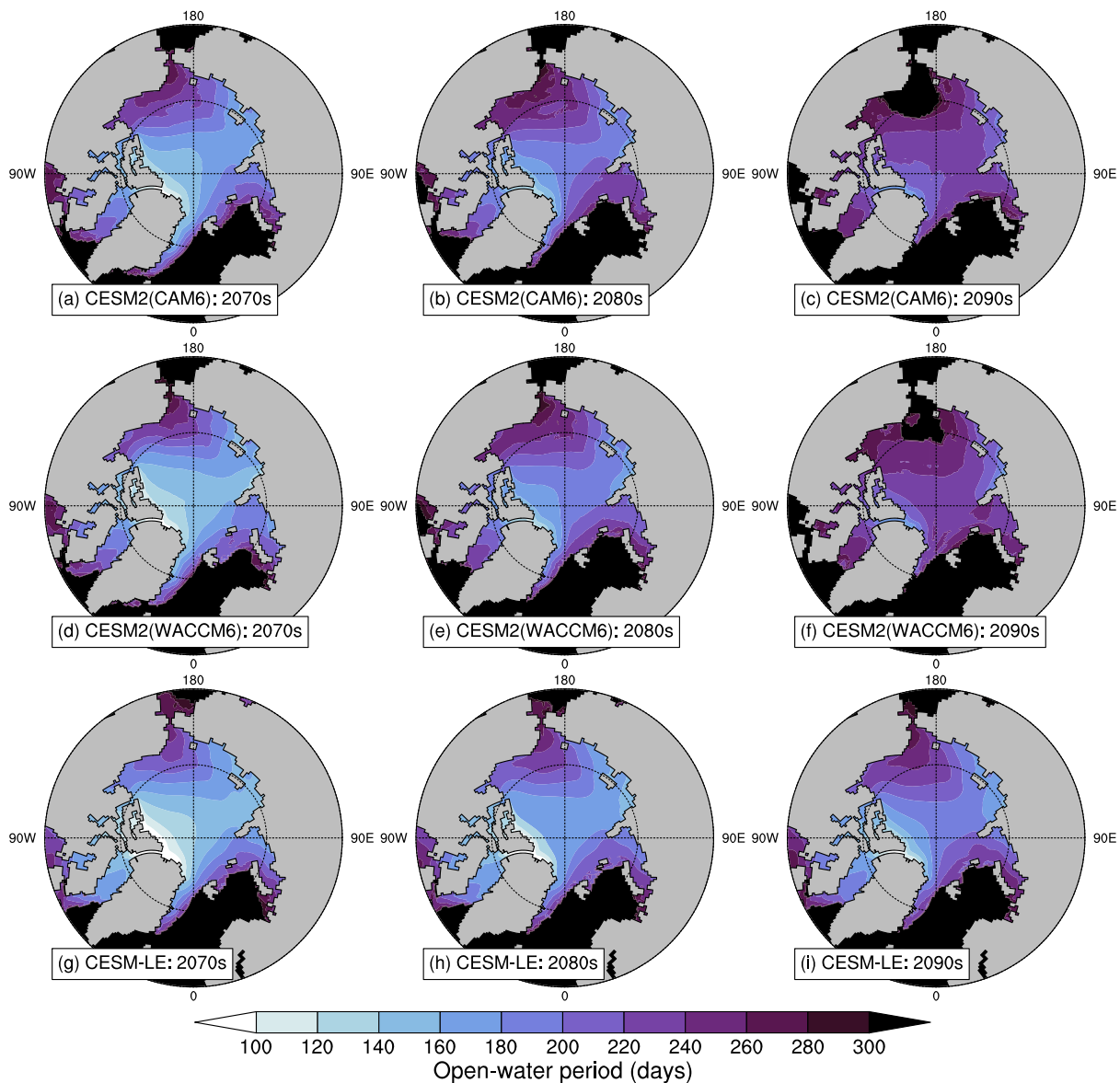
Figure 11. Ensemble mean, decadal mean length of the open-water period during the 2070s (a, d, g), 2080s (b, e, h), and 2090s (c, f, i) in the CESM2(CAM6) (a–c), the CESM2(WACCM6) (d–f), and the CESM-LE (g–i).

trends are largest (not shown). September sea ice volume trends also show a similar pattern as sea ice area (Figure S4). This implies that the Arctic sea ice cover is also not thinning over this period, in addition to no loss in ice area. The cause of the reduced negative trends in ice area and volume is currently unknown and requires further work beyond the scope of this paper. Nevertheless, it is important to highlight this feature of the CESM2 simulations here, as it may impact other aspects of the Arctic and global climate in the CESM2. While we do not currently know the cause of this pattern, we have been able to rule out a few possible explanations.

Although natural climate variability can cause positive 20-year trends in Arctic sea ice (Kay et al., 2011), we find that the change in the CESM2 trends is likely not the result of internal variability, given that all ensemble members from all CMIP6 scenarios show such a pattern (Figure 12). We have also ruled out a number of forcings as the cause of the pattern in the trends. In particular, we calculated the same 20-year linear trends in September sea ice area and volume using the AerChemMIP hist-piNTCF (Danabasoglu, 2019g), hist-1950HC (Danabasoglu, 2019f), and SSP3-7.0-lowNTCF (Danabasoglu, 2019h) simulations and found similar results
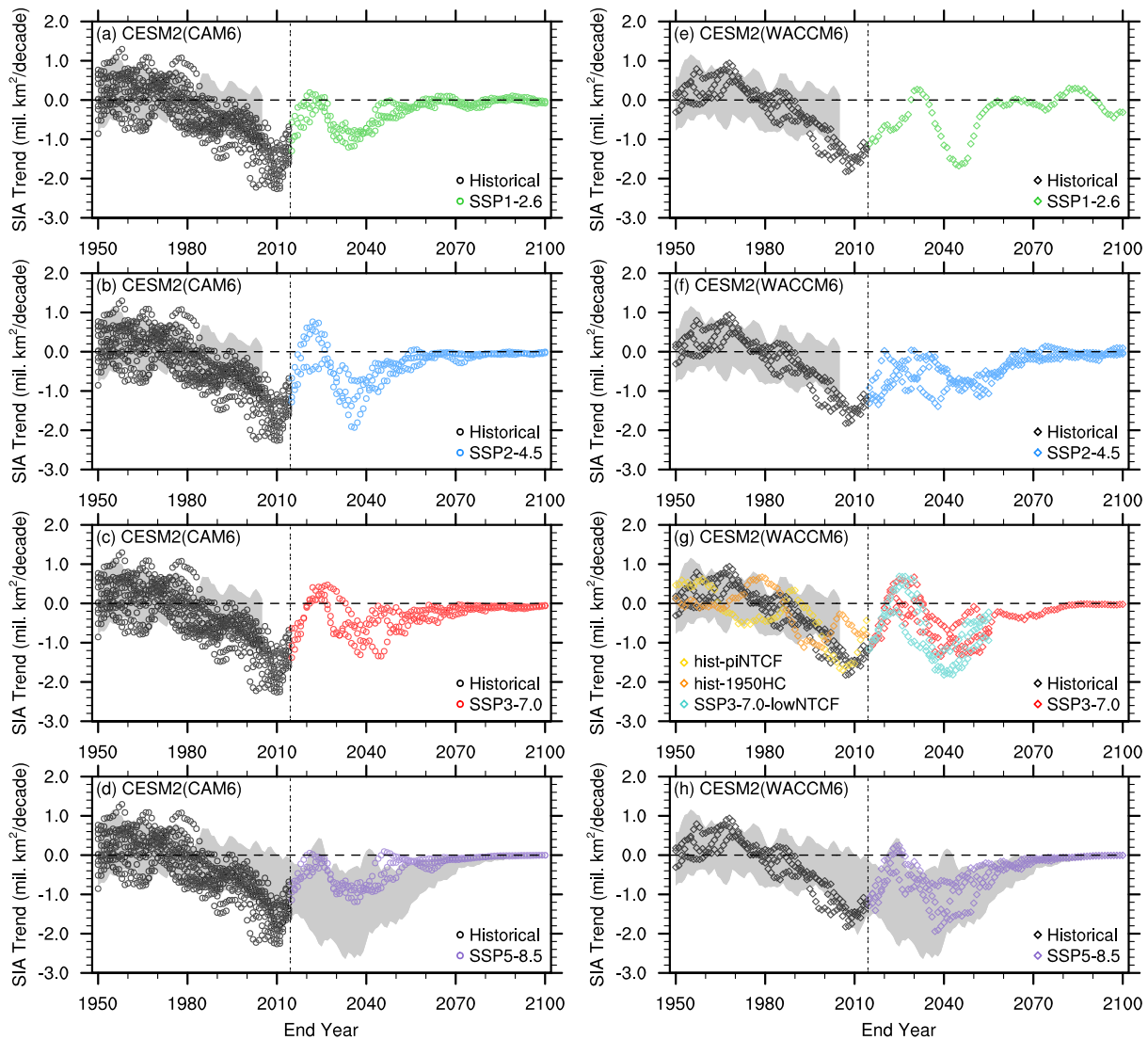
Figure 12. Twenty-year linear trends in September ice area in the CESM2(CAM6) (a–d) and the CESM2(WACCM6) (e–h) under the historical forcing (black) and different future emissions scenarios (colors). Panel (g) also includes 20-year linear trends in September ice area from three AerChemMIP experiments (Collins et al., 2017). The range of trends in September ice area across all ensemble members of the CESM-LE (gray shading) is shown for the historical period in all panels and additionally for the RCP8.5 scenario in panels (d) and (h). Values on the *x* axis indicate the end year of the 20-year period over which linear trends are calculated. The horizontal dashed lines indicate no trend, and the vertical double-dashed lines indicate the transition year between historical and future simulations in the CESM2.

(Figures 12g and S4g). The AerChemMIP simulations use WACCM6 as their atmospheric component and are meant to quantify the effect of chemistry and aerosols in CMIP6 (as described in Collins et al., 2017). The hist-piNTCF simulation covers the historical period 1850–2014, with emissions of near-term climate forcers (NTCFs: methane, tropospheric ozone and aerosols, and their precursors) fixed at preindustrial levels at the start of the simulation. The hist-1950HC simulation also covers the historical period 1850–2014 and branches from the CMIP6 historical simulation at year 1950 with chlorofluorocarbon (CFC) and hydrochlorofluorocarbon (HCFC) concentrations fixed at 1950 conditions, resulting in a 20th century climate without an ozone hole. The two AerChemMIP historical simulations show a stabilization of the trends in ice area toward the end of the historical period, similar to the CESM2(WACCM6) historical simulations (Figure 12g). Therefore, these particular forcings are likely not the cause for the stabilization of the trends in ice area at the end of the historical period. The SSP3-7.0-lowNTCF simulations start at the end of the historical simulations and are branched from the three CESM2(WACCM6) historical ensemble

members. They are run for 41 years following the SSP3-7.0-lowNTCF scenario, a version of the SSP3-7.0 scenario with cleaner air quality policies. All three ensemble members show a similar behavior during the first 10–15 years of the future simulations as the three CESM2(WACCM6) SSP3-7.0 ensemble members (Figure 12g), indicating that the specific aerosol and ozone precursors that are kept at a "clean" level are likely not the cause of the change in trends either. Finally, given that anthropogenic and biomass burning secondary organic aerosol emissions were set to zero from 2015 onward in the initial CESM2(CAM6) future scenario simulations (see section 2.1 for more details) and that these simulations also showed this trend behavior (not shown), the anthropogenic and biomass burning secondary organic aerosol emissions can also be ruled out as a possible explanation for this pattern in the trends.

7. Conclusions

In this contribution, we presented an analysis of some key metrics of the historical and future simulations from two configurations of the CESM2 compared to its previous version, the CESM-LE, as well as observations. We found that the winter ice thickness distribution of the CESM2(CAM6) configuration is biased thin over the historical period, which leads to lower September sea ice area compared to the CESM2(WACCM6), the CESM-LE, and observations. As a result, the CESM2(CAM6) generally reaches first September ice-free conditions earlier than the CESM2(WACCM6) and the CESM-LE. The timing of first September ice-free conditions in the Arctic is found to be insensitive to the choice of CMIP6 future emissions scenario in both CESM2 configurations. Instead, the first year of an ice-free September is determined by internal variability, with the CESM2 showing a two to three decade uncertainty range, similar to the two decades found in the CESM-LE (Jahn et al., 2016). Regarding the response of Arctic sea ice to global warming, the CESM2 simulates a low probability of ice-free conditions in September if warming is limited to 1.5°C but increases for any additional warming, consistent with previous studies (Jahn, 2018; Sanderson et al., 2017; Screen & Williamson, 2017; Sigmond et al., 2018). By the late 21st century, the CESM2 exhibits an accelerated decline in winter and spring ice area that was not sampled in the CESM-LE simulations. However, when looking at the evolution of March ice area as a function of atmospheric CO_2 or Arctic temperature rather than time, the two versions of the CESM model are consistent and the differences in their time evolution arise as the CESM2 reaches higher CO_2 concentrations and Arctic temperatures than those in the CESM-LE. Our results suggest that reaching CO_2 concentration higher than 900 ppm and annual mean Arctic temperatures higher than −4°C could lead to an accelerated loss of winter and spring sea ice in the Arctic. The different simulated climate by 2100 between the CESM1 simulations with CMIP5 forcing versus the CESM2 simulations with CMIP6 forcing results in less ocean heat loss during the fall months in the CESM2. This strongly delays the formation of sea ice by keeping the surface temperature of the ocean above freezing point for a longer period of time and leads to ice-free conditions for up to 8 months of the year in the CESM2 and an open-water period more than 30 days longer than in the CESM-LE. It is important to note that the evolution of March ice area is not as consistent between the CESM-LE and the CESM2 when analyzed as a function of temperature anomaly rather than absolute temperature due to differences in the mean global temperature of the reference period (McIlhattan et al., 2020). This highlights the need for caution when comparing model versions in terms of temperature anomaly, something that is widely done when analyzing the potential impacts of global warming.

We also document a large reduction in the simulated 20-year linear trends in September ice conditions, indicating less rapid ice loss and thinning, around the transition between historical and future simulations in the CESM2. This feature is consistent across both CESM2 configurations, all ensemble members, and all future scenarios considered here and is also present in all months of the year. Based on preliminary analysis in section 6, we have ruled out the following explanations for this behavior: internal variability, NTCFs and their precursors, CFCs and HCFCs, as well as anthropogenic and biomass burning secondary organic aerosol emissions. More analysis is needed to understand the causes and implications of this pattern in the Arctic sea ice trends.

To conclude, our analysis provides the first overview of the major features of the evolution of Arctic sea ice in the CESM2 over the 20th and 21st centuries. Overall, the CESM2 reasonably simulates the important properties of Arctic sea ice, with the CESM2(WACCM6) generally performing better than the CESM2(CAM6) over the historical period. Differences in the simulated sea ice between the two CESM2 configurations, and

differences compared to the previous version (CESM-LE), are important to consider when analyzing other aspects of these new CMIP6 simulations, in particular in the Arctic. An important bias to keep in mind for future work involving the CESM2 is the lower-than-observed mean state of Arctic sea ice in the CESM2(CAM6) during the historical period, which results in simulated September ice-free conditions as early as 2010. Biased simulations of present-day sea ice properties, especially Arctic sea ice volume, have been shown to bias future projections of summer sea ice conditions (Massonnet et al., 2018). This suggests that the CESM2(WACCM6), with its present-day Arctic sea ice mean state closer to observations, is the more appropriate CESM2 configuration contributed to CMIP6 to use for in-depth studies of future sea ice changes in the Arctic.

Data Availability Statement

Previous and current versions of the CESM are freely available at www.cesm.ucar.edu/models/?ref=hp. The CESM2 data analyzed in this study have been contributed to CMIP6 and are freely available from the Earth System Grid Federation (ESGF) at https://esgf-node.llnl.gov/search/cmip6/, from the NCAR Digital Asset Services Hub (DASH) at data.ucar.edu, and from the links provided on the CESM website at www.cesm.ucar.edu/models/cesm2/. Note that we here use the corrected CESM2(CAM6) future scenario simulations, uploaded to the CMIP6 archive in May 2020. The CESM-LE data can be found at www.cesm.ucar.edu/projects/community-projects/LENS/.

References

Assur, A. (1960). *Composition of sea ice and its tensile strength* (Vol. 44). US Army Snow, Ice and Permafrost Research Establishment.

Barnhart, K. R., Miller, C. R., Overeem, I., & Kay, J. E. (2016). Mapping the future expansion of Arctic open water. *Nature Climate Change*, *6*(3), 280. https://doi.org/10.1038/NCLIMATE2848

Bitz, C. M., & Lipscomb, W. H. (1999). An energy-conserving thermodynamic model of sea ice. *Journal of Geophysical Research*, *104*(C7), 15,669–15,677. https://doi.org/10.1029/1999JC900100

Bitz, C. M., & Roe, G. H. (2004). A mechanism for the high rate of sea ice thinning in the Arctic Ocean. *Journal of Climate*, *17*(18), 3623–3632. https://doi.org/10.1175/1520-0442(2004)017<3623:AMFTHR>2.0.CO;2

Bliss, A. C., Steele, M., Peng, G., Meier, W. N., & Dickinson, S. (2019). Regional variability of Arctic sea ice seasonal change climate indicators from a passive microwave climate data record. *Environmental Research Letters*, *14*, 045003. https://doi.org/10.1088/1748-9326/aafb84

Bunzel, F., Notz, D., & Pedersen, L. T. (2018). Retrievals of Arctic sea-ice volume and its trend significantly affected by interannual snow variability. *Geophysical Research Letters*, *45*, 11,751–11,759. https://doi.org/10.1029/2018GL078867

Chevallier, M., Smith, G. C., Dupont, F., Lemieux, J.-F., Forget, G., Fujii, Y., et al. (2017). Intercomparison of the Arctic sea ice cover in global ocean-sea ice reanalyses from the ORA-IP project. *Climate Dynamics*, *49*(3), 1107–1136. https://doi.org/10.1007/s00382-016-2985-y

Collins, W. J., Lamarque, J.-F., Schulz, M., Boucher, O., Eyring, V., Hegglin, M. I., et al. (2017). AerChemMIP: Quantifying the effects of chemistry and aerosols in CMIP6. *Geoscientific Model Development*, *10*(2), 585–607. https://doi.org/10.5194/gmd-10-585-2017

Comiso, J. C., Meier, W. N., & Gersten, R. (2017). Variability and trends in the Arctic sea ice cover: Results from different techniques. *Journal of Geophysical Research: Oceans*, *122*, 6883–6900. https://doi.org/10.1002/2017JC012768

Danabasoglu, G. (2019a). NCAR CESM2 model output prepared for CMIP6 CMIP historical. https://doi.org/10.22033/ESGF/CMIP6.7627

Danabasoglu, G. (2019b). NCAR CESM2 model output prepared for CMIP6 ScenarioMIP ssp126. https://doi.org/10.22033/ESGF/CMIP6.7746

Danabasoglu, G. (2019c). NCAR CESM2 model output prepared for CMIP6 ScenarioMIP ssp245. https://doi.org/10.22033/ESGF/CMIP6.7748

Danabasoglu, G. (2019d). NCAR CESM2 model output prepared for CMIP6 ScenarioMIP ssp370. https://doi.org/10.22033/ESGF/CMIP6.7753

Danabasoglu, G. (2019e). NCAR CESM2 model output prepared for CMIP6 ScenarioMIP ssp585. https://doi.org/10.22033/ESGF/CMIP6.7768

Danabasoglu, G. (2019f). NCAR CESM2-WACCM model output prepared for CMIP6 AerChemMIP hist-1950HC. https://doi.org/10.22033/ESGF/CMIP6.10060

Danabasoglu, G. (2019g). NCAR CESM2-WACCM model output prepared for CMIP6 AerChemMIP hist-piNTCF. https://doi.org/10.22033/ESGF/CMIP6.10062

Danabasoglu, G. (2019h). NCAR CESM2-WACCM model output prepared for CMIP6 AerChemMIP ssp370-lowNTCF. https://doi.org/10.22033/ESGF/CMIP6.10104

Danabasoglu, G. (2019i). NCAR CESM2-WACCM model output prepared for CMIP6 CMIP historical. https://doi.org/10.22033/ESGF/CMIP6.10071

Danabasoglu, G. (2019j). NCAR CESM2-WACCM model output prepared for CMIP6 ScenarioMIP ssp126. https://doi.org/10.22033/ESGF/CMIP6.10100

Danabasoglu, G. (2019k). NCAR CESM2-WACCM model output prepared for CMIP6 ScenarioMIP ssp245. https://doi.org/10.22033/ESGF/CMIP6.10101

Danabasoglu, G. (2019l). NCAR CESM2-WACCM model output prepared for CMIP6 ScenarioMIP ssp370. https://doi.org/10.22033/ESGF/CMIP6.10102

Danabasoglu, G. (2019m). NCAR CESM2-WACCM model output prepared for CMIP6 ScenarioMIP ssp585. https://doi.org/10.22033/ESGF/CMIP6.10115

Danabasoglu, G., Bates, S. C., Briegleb, B. P., Jayne, S. R., Jochum, M., Large, W. G., et al. (2012). The CCSM4 ocean component. *Journal of Climate*, *25*(5), 1361–1389. https://doi.org/10.1175/JCLI-D-11-00091.1

Danabasoglu, G., Lamarque, J.-F., Bacmeister, J., Bailey, D. A., DuVivier, A. K., Edwards, J., et al. (2020). The Community Earth System Model version 2 (CESM2). *Journal of Advances in Modeling Earth Systems*, *12*, e2019MS001916. https://doi.org/10.1029/2019MS001916

DeRepentigny, P., Tremblay, L. B., Newton, R., & Pfirman, S. (2016). Patterns of sea ice retreat in the transition to a seasonally ice-free Arctic. *Journal of Climate*, *29*(19), 6993–7008. https://doi.org/10.1175/JCLI-D-15-0733.1

DuVivier, A. K., Holland, M. M., Kay, J. E., Tilmes, S., Gettelman, A., & Bailey, D. (2020). Arctic and Antarctic sea ice mean state in the Community Earth System Model version 2 and the influence of atmospheric chemistry. *Journal of Geophysical Research: Oceans*, *125*, e2019JC015934. https://doi.org/10.1029/2019JC015934

England, M., Jahn, A., & Polvani, L. (2019). Nonuniform contribution of internal variability to recent Arctic sea ice loss. *Journal of Climate*, *32*(13), 4039–4053. https://doi.org/10.1175/JCLI-D-18-0864.1

Eyring, V., Bony, S., Meehl, G. A., Senior, C. A., Stevens, B., Stouffer, R. J., & Taylor, K. E. (2016). Overview of the Coupled Model Intercomparison Project Phase 6 (CMIP6) experimental design and organization. *Geoscientific Model Development (Online)*, *9*(LLNL-JRNL-736881), 1937–1958.

Fernández-Méndez, M., Katlein, C., Rabe, B., Nicolaus, M., Peeken, I., Bakker, K., et al. (2015). Photosynthetic production in the central Arctic Ocean during the record sea-ice minimum in 2012. *Biogeosciences*, *12*(11), 3525–3549. https://doi.org/10.5194/bg-12-3525-2015

Fetterer, F., Knowles, K., Meier, W. N., Savoie, M., & Windnagel, A. K. (2017). Sea Ice Index, Version 3 [monthly values from 1979 to 2020]. National Snow and Ice Data Center, Boulder, Colorado, USA, accessed May 2020.

Gettelman, A., Hannay, C., Bacmeister, J. T., Neale, R. B., Pendergrass, A. G., Danabasoglu, G., et al. (2019). High climate sensitivity in the Community Earth System Model version 2 (CESM2). *Geophysical Research Letters*, *46*, 8329–8337. https://doi.org/10.1029/2019GL083978

Gettelman, A., Mills, M. J., Kinnison, D. E., Garcia, R. R., Smith, A. K., Marsh, D. R., et al. (2019). The Whole Atmosphere Community Climate Model Version 6 (WACCM6). *Journal of Geophysical Research: Atmospheres*, *124*, 12,380–12,403. https://doi.org/10.1029/2019JD030943

Gillett, N. P., Arora, V. K., Zickfeld, K., Marshall, S. J., & Merryfield, W. J. (2011). Ongoing climate change following a complete cessation of carbon dioxide emissions. *Nature Geoscience*, *4*(2), 83–87. https://doi.org/10.1038/ngeo1047

Hunke, E. C., Hebert, D. A., & Lecomte, O. (2013). Level-ice melt ponds in the Los Alamos sea ice model, CICE. *Ocean Modelling*, *71*, 26–42. https://doi.org/10.1016/j.ocemod.2012.11.008

Hunke, E. C., Lipscomb, W. H., Turner, A. K., Jeffery, N., & Elliot, S. (2015). CICE: The Los Alamos Sea Ice Model documentation and software user's manual version 5.1 (*LA-CC-06-012*): Los Alamos National Laboratory.

Hurrell, J. W., Holland, M. M., Gent, P. R., Ghan, S., Kay, J. E., Kushner, P. J., et al. (2013). The Community Earth System Model: A framework for collaborative research. *Bulletin of the American Meteorological Society*, *94*(9), 1339–1360. https://doi.org/10.1175/BAMS-D-12-00121.1

Jahn, A. (2018). Reduced probability of ice-free summers for 1.5°C compared to 2°C warming. *Nature Climate Change*, *8*(5), 409. https://doi.org/10.1038/s41558-018-0127-8

Jahn, A., Kay, J. E., Holland, M. M., & Hall, D. M. (2016). How predictable is the timing of a summer ice-free Arctic? *Geophysical Research Letters*, *43*, 9113–9120. https://doi.org/10.1002/2016GL070067

Kay, J. E., Deser, C., Phillips, A., Mai, A., Hannay, C., Strand, G., et al. (2015). The Community Earth System Model (CESM) large ensemble project: A community resource for studying climate change in the presence of internal climate variability. *Bulletin of the American Meteorological Society*, *96*(8), 1333–1349. https://doi.org/10.1175/BAMS-D-13-00255.1

Kay, J. E., Holland, M. M., & Jahn, A. (2011). Inter-annual to multi-decadal Arctic sea ice extent trends in a warming world. *Geophysical Research Letters*, *38*, L15708. https://doi.org/10.1029/2011GL048008

Kirchmeier-Young, M. C., Zwiers, F. W., & Gillett, N. P. (2017). Attribution of extreme events in Arctic sea ice extent. *Journal of Climate*, *30*(2), 553–571. https://doi.org/10.1175/JCLI-D-16-0412.1

Kwok, R. (2018). Arctic sea ice thickness, volume, and multiyear ice coverage: Losses and coupled variability (1958–2018). *Environmental Research Letters*, *13*(10), 105005. https://doi.org/10.1088/1748-9326/aae3ec

Labe, Z., Magnusdottir, G., & Stern, H. (2018). Variability of Arctic sea ice thickness using PIOMAS and the CESM Large Ensemble. *Journal of Climate*, *31*(8), 3233–3247. https://doi.org/10.1175/JCLI-D-17-0436.1

Lawrence, D. M., Fisher, R. A., Koven, C. D., Oleson, K. W., Swenson, S. C., Bonan, G., et al. (2019). The Community Land Model version 5: Description of new features, benchmarking, and impact of forcing uncertainty. *Journal of Advances in Modeling Earth Systems*, *11*, 4245–4287. https://doi.org/10.1029/2018MS001583

Massonnet, F., Vancoppenolle, M., Goosse, H., Docquier, D., Fichefet, T., & Blanchard-Wrigglesworth, E. (2018). Arctic sea-ice change tied to its mean state through thermodynamic processes. *Nature Climate Change*, *8*(7), 599. https://doi.org/10.1038/s41558-018-0204-z

McIlhattan, E. A., Kay, J. E., & L'Ecuyer, T. S. (2020). Arctic clouds and precipitation in the Community Earth System Model version 2. *Journal of Geophysical Research: Atmospheres*. https://doi.org/10.1029/2020JD032521

Meehl, G. A., Arblaster, J. M., Bates, S., Tebaldi, C., Shields, C., Richter, J. H., et al. (2020). Characteristics of future warmer base states in CESM2. *Earth and Space Science*, *7*, e2020EA001296. https://doi.org/10.1029/2020EA001296

Meier, W. N., Fetterer, F., Savoie, M., Mallory, S., Duerr, R., & Stroeve, J. C. (2017). NOAA/NSIDC Climate Data Record of Passive Microwave Sea Ice Concentration, Version 3 [September averages 1980 to 2009]. https://doi.org/10.7265/N59P2ZTG

Moore, S. E., & Huntington, H. P. (2008). Arctic marine mammals and climate change: Impacts and resilience. *Ecological Applications*, *18*(sp2), S157–S165. https://doi.org/10.1890/06-0571.1

Notz, D. (2014). Sea-ice extent and its trend provide limited metrics of model performance. *The Cryosphere*, *8*, 229–243.

Notz, D., Jahn, A., Holland, M., Hunke, E., Massonnet, F., Stroeve, J., et al. (2016). The CMIP6 Sea-Ice Model Intercomparison Project (SIMIP): Understanding sea ice through climate-model simulations. *Geoscientific Model Development (Online)*, *9*(LA-UR-16-25878), 3427–3446. https://doi.org/10.5194/gmd-9-3427-2016

O'Neill, B. C., Kriegler, E., Riahi, K., Ebi, K. L., Hallegatte, S., Carter, T. R., et al. (2014). A new scenario framework for climate change research: The concept of shared socioeconomic pathways. *Climatic Change*, *122*(3), 387–400. https://doi.org/10.1007/s10584-013-0905-2

O'Neill, B. C., Tebaldi, C., Vuuren, D. P., Eyring, V., Friedlingstein, P., Hurtt, G., et al. (2016). The Scenario Model Intercomparison Project (ScenarioMIP) for CMIP6. *Geoscientific Model Development*, *9*(9), 3461–3482. https://doi.org/10.5194/gmd-9-3461-2016

Parkinson, C. L. (2014). Spatially mapped reductions in the length of the Arctic sea ice season. *Geophysical Research Letters*, *41*, 4316–4322. https://doi.org/10.1002/2014GL060434

Peng, G., Meier, W. N., Scott, D. J., & Savoie, M. H. (2013). A long-term and reproducible passive microwave sea ice concentration data record for climate studies and monitoring. *Earth System Science Data*, *5*(2), 311–318. https://doi.org/10.5194/essd-5-311-2013

Perovich, D. K., Nghiem, S. V., Markus, T., & Schweiger, A. (2007). Seasonal evolution and interannual variability of the local solar energy absorbed by the Arctic sea ice–ocean system. *Journal of Geophysical Research*, *112*, C03005. https://doi.org/10.1029/2006JC003558

Post, E., Bhatt, U. S., Bitz, C. M., Brodie, J. F., Fulton, T. L., Hebblewhite, M., et al. (2013). Ecological consequences of sea-ice decline. *Science*, *341*(6145), 519–524. https://doi.org/10.1126/science.1235225

SIMIP Community (2020). Arctic sea ice in CMIP6. *Geophysical Research Letters*, *47*, e2019GL086749. https://doi.org/10.1029/2019GL086749

Sanderson, B. M., Xu, Y., Tebaldi, C., Wehner, M., O'Neill, B. C., Jahn, A., et al. (2017). Community climate simulations to assess avoided impacts in 1.5 and 2°C futures. *Earth System Dynamics*, *8*(3), 827–847. https://doi.org/10.3929/ethz-b-000191578

Screen, J. A. (2018). Arctic sea ice at 1.5 and 2°C. *Nature Climate Change*, *8*(5), 362–363. https://doi.org/10.1038/s41558-018-0137-6

Screen, J. A., & Williamson, D. (2017). Ice-free Arctic at 1.5°C? *Nature Climate Change*, *7*(4), 230. https://doi.org/10.1038/nclimate3248

Sigmond, M., Fyfe, J. C., & Swart, N. C. (2018). Ice-free Arctic projections under the Paris Agreement. *Nature Climate Change*, *8*(5), 404. https://doi.org/10.1038/s41558-018-0124-y

Smith, A., & Jahn, A. (2019). Definition differences and internal variability affect the simulated Arctic sea ice melt season. *The Cryosphere*, *13*(1), 1–20. https://doi.org/10.5194/tc-13-1-2019

Smith, R., Jones, P., Briegleb, B., Bryan, F., Danabasoglu, G., Dennis, J., et al. (2010). The Parallel Ocean Program (POP) reference manual: Ocean component of the Community Climate System Model (CCSM) and Community Earth System Model (CESM). *Rep. LAUR-01853*, *141*, 1–140.

Stroeve, J. C., Markus, T., Boisvert, L., Miller, J., & Barrett, A. (2014). Changes in Arctic melt season and implications for sea ice loss. *Geophysical Research Letters*, *41*, 1216–1225. https://doi.org/10.1002/2013GL058951

Stroeve, J., & Notz, D. (2018). Changing state of Arctic sea ice across all seasons. *Environmental Research Letters*, *13*(10), 103001. https://doi.org/10.1088/1748-9326/aade56

Swart, N. C., Fyfe, J. C., Hawkins, E., Kay, J. E., & Jahn, A. (2015). Influence of internal variability on Arctic sea-ice trends. *Nature Climate Change*, *5*(2), 86. https://doi.org/10.1038/nclimate2483

Tilmes, S., Hodzic, A., Emmons, L. K., Mills, M. J., Gettelman, A., Kinnison, D. E., et al. (2019). Climate forcing and trends of organic aerosols in the Community Earth System Model (CESM2). *Journal of Advances in Modeling Earth Systems*, *11*, 4323–4351. https://doi.org/10.1029/2019MS001827

Turner, A. K., & Hunke, E. C. (2015). Impacts of a mushy-layer thermodynamic approach in global sea-ice simulations using the CICE sea-ice model. *Journal of Geophysical Research: Oceans*, *120*, 1253–1275. https://doi.org/10.1002/2014JC010358

Van Vuuren, D. P., Edmonds, J., Kainuma, M., Riahi, K., Thomson, A., Hibbard, K., et al. (2011). The representative concentration pathways: An overview. *Climatic Change*, *109*(1–2), 5. https://doi.org/10.1007/s10584-011-0148-z

Wang, M., Yang, Q., Overland, J. E., & Stabeno, P. (2018). Sea-ice cover timing in the Pacific Arctic: The present and projections to mid-century by selected CMIP5 models. *Deep Sea Research Part II: Topical Studies in Oceanography*, *152*, 22–34. https://doi.org/10.1016/j.dsr2.2017.11.017

Erratum

Following the publication of this article, the authors discovered that, contrary to standard protocol, NCAR continued historical ensemble members 10, 11, and 4 as the future CESM2(CAM6) runs after 2014, not members 1, 2, and 3 as is the case for the future CESM2(WACCM6) runs. Consequently, the match between historical and future scenario runs between years 2014 and 2015 was incorrect in the originally published paper, which affected Figures 3, 12, and S4. These figures have been replaced with versions that line up the historical and future runs correctly; small changes were made to the markers around years 2015-2033 in Figures 12a-d and S4a-d and to the solid and dotted orange lines in the histogram in Figure 3d. Those changes do not impact any of the conclusions. This may be considered the official version of record.